

Heat transport in Rayleigh–Bénard convection and angular momentum transport in Taylor–Couette flow: a comparative study

Hannes Brauckmann,¹ Bruno Eckhardt,^{1,2} and Jörg Schumacher³

¹*Fachbereich Physik, Philipps-Universität Marburg, D-35032 Marburg, Germany*

²*J. M. Burgerscentrum, Delft University of Technology, 2628 CD Delft, The Netherlands*

³*Institut für Thermo- und Fluidodynamik, Technische Universität Ilmenau,
Postfach 100565, D-98684 Ilmenau, Germany*

(Dated: February 12, 2022)

Abstract

Rayleigh–Bénard convection and Taylor–Couette flow are two canonical flows that have many properties in common. We here compare the two flows in detail for parameter values where the Nusselt numbers, i.e. the thermal transport and the angular momentum transport normalized by the corresponding laminar values, coincide. We study turbulent Rayleigh–Bénard convection in air at Rayleigh number $Ra = 10^7$ and Taylor–Couette flow at shear Reynolds number $Re_S = 2 \times 10^4$ for two different mean rotation rates but the same Nusselt numbers. For individual pairwise related fields and convective currents, we compare the probability density functions normalized by the corresponding root mean square values and taken at different distances from the wall. We find one rotation number for which there is very good agreement between the mean profiles of the two corresponding quantities temperature and angular momentum. Similarly, there is good agreement between the fluctuations in temperature and velocity components. For the heat and angular momentum currents, there are differences in the fluctuations outside the boundary layers that increase with overall rotation and can be related to differences in the flow structures in the boundary layer and in the bulk. The study extends the similarities between the two flows from global quantities to local quantities and reveals the effects of rotation on the transport.

I. INTRODUCTION

Convection in layers of fluids heated from below and cooled from above (Rayleigh–Bénard or RB flow) and the flow between two rotating cylinders (Taylor–Couette or TC flow) are among the canonical flows in fluid mechanics. Studies of their stability properties and the manner in which the laminar profiles give way to more structured and complicated flows have provided much insight into the transition to turbulence with linear instabilities [8, 17]. The behavior well above the onset of turbulence has also been investigated starting with the experiments by Wendt [28]. Many different flow regimes that are not yet fully explained or explored have been described [16, 23]. It was realized early on that despite the differences in the driving forces, there are many similarities, and it is helpful to draw analogies and to compare the properties of both flows [18]. The intimate relations between the two flows have led Busse [6] to characterize them as the *twins of turbulence*.

A formal analogy between RB and TC flow (and pipe flow as well) was developed and described in Eckhardt et al. [12, 13] (see also Bradshaw [2] for an earlier approximate relation and Dubrulle & Hersant [11] for a similar analogy). The analogy identifies pairs of equations that describe the total energy dissipation and the global transport of heat or angular momentum, respectively, in the two flows. The equations allow one to relate transport properties, dimensionless parameters and other quantities, and have been used in particular to study scaling relations in fully developed turbulent flows [16]. The similarity in the equations suggests that a more detailed comparison between the two flows should be possible.

We here explore this option within direct numerical simulations (DNS). We describe the difficulties one has to overcome in identifying corresponding parameters, and present case studies where detailed comparisons are possible. In particular, we will compare the turbulent transport currents with respect to their statistical properties. Furthermore, we can relate components of the involved turbulent fields to each other and compare their statistical fluctuations at different distances from the walls. The focus of our study is on the general ideas and an illustration for a few examples, but not on a comprehensive study for all parameter values. Specifically, we will take one set of data for RB flow and compare it to TC flow cases at two different rotation numbers, which allows us to study the effect of rotation. The data are taken from well-resolved DNS of both flows at moderate Rayleigh and Reynolds numbers.

The outline of the manuscript is as follows. In section II we present the balance equations, the numerical methods and discuss the analogy. In section III the choice of corresponding parameters for the comparison is explained. In section IV the area-averaged mean currents and their probability density functions (PDFs) as well as other pairwise related properties at different distances from the wall are analyzed. We conclude the work with a short discussion of the particular structures of the

convective currents and a summary in section V.

II. RELATIONS FOR TRANSPORT CURRENTS AND DISSIPATION RATES

RB flow is modeled by the three-dimensional Boussinesq equations for the velocity field \mathbf{u} and the temperature field T [1, 9]. The equations are solved using the Nek5000 software [21], a spectral element method [15, 25]. The physical system is characterized by the imposed temperature difference between bottom and top plates, Δ , the height d of the domain, and the free-fall velocity $U_f = \sqrt{g\alpha\Delta d}$ with the thermal expansion coefficient α and the acceleration due to gravity, g . The kinematic viscosity ν of the fluid and the thermal diffusivity κ are combined in the Prandtl number $Pr = \nu/\kappa$. The flow is confined to a cylinder with insulating sidewalls.

The mean heat flux across the layer, i.e., in the z -direction, is given by

$$J_T = \langle u_z T \rangle - \kappa \frac{\partial \langle T \rangle}{\partial z} = Nu_T J_{T,lam}, \quad (1)$$

with $J_{T,lam}$ the purely diffusive heat flux below the onset of convective motion,

$$J_{T,lam} = \kappa \frac{\Delta}{d}. \quad (2)$$

Here, $\langle \cdot \rangle = \langle \cdot \rangle_{A,t}$ denotes an average over horizontal planes at fixed height and over time. Equation (1) already contains the definition of the Nusselt number Nu_T which measures the heat transport relative to the laminar situation. A second relevant equation is that for the mean kinetic energy dissipation rate of the velocity field ϵ_u . It is obtained by multiplying the momentum balance of the Navier–Stokes–Boussinesq equations with the velocity \mathbf{u} and integrating over the volume and over time,

$$\epsilon_u = \frac{\nu^3}{d^4} Pr^{-2} Ra (Nu_T - 1). \quad (3)$$

Here, $Ra = \alpha g d^3 \Delta / (\kappa \nu)$ is the Rayleigh number, the second dimensionless parameter. The data set which we use for the comparisons is obtained in a closed cylindrical cell with a unity aspect ratio (diameter=height) at $Ra = 10^7$ and $Pr = 0.7$.

The TC system is characterised by the radii r_1 and r_2 of the inner and outer cylinder, which rotate with the angular velocities ω_1 and ω_2 , respectively. The flow between the cylinders is governed by the incompressible Navier–Stokes equations for the velocity $\mathbf{u} = (u_r, u_\varphi, u_z)$ in cylindrical coordinates (r, φ, z) . We solve the equations with periodic boundary conditions in the axial direction using a spectral method [20]. In TC flow, the gap width $d = r_2 - r_1$ and the velocity difference between the cylinders $U_0 = 2r_1 r_2 (r_1 + r_2)^{-1} (\omega_1 - \omega_2)$ (calculated in a rotating frame of reference [5, 10]) serve as characteristic scales for lengths and velocities. We choose a system height of $2d$ so that one pair of

Taylor vortices fits into the computational domain. Thus, the diameter of a single Taylor vortex is similar to that of the large-scale circulation in RB flow with aspect ratio one. Further details of the simulation procedure are discussed in references [3, 5].

For the derivation of expressions in TC flow that correspond to (1) and (3) in RB flow, we start with the azimuthal velocity u_φ . Averaging the φ -component of the Navier–Stokes equation over time and over cylinders at fixed radii r between the positions of the inner (r_1) and outer (r_2) cylinder, one finds [12, 13]

$$J_\omega = r^3 \left(\langle u_r \omega \rangle - \nu \frac{\partial \langle \omega \rangle}{\partial r} \right) = Nu_\omega J_{\omega, lam}, \quad (4)$$

with the angular velocity $\omega = u_\varphi/r$ and $J_{\omega, lam}$ the angular momentum flux in the laminar case,

$$J_{\omega, lam} = \nu \frac{r_1^2 r_2^2}{r_a d} (\omega_1 - \omega_2). \quad (5)$$

Here, $r_a = (r_1 + r_2)/2$ is the mean radius. The averaged current J_ω is independent of the radius and conserved in time. Physically, it corresponds to the torque needed to keep the cylinders in motion; it corresponds naturally to the heat transport (1) in RB flow, which is why we also introduced a Nusselt number Nu_ω corresponding to Nu_T . Similarly, one can multiply the Navier–Stokes equation with the velocity \mathbf{u} and average over volume and time to obtain the mean kinetic energy dissipation rate, corresponding to (3). However, the dissipation associated with the laminar profile has to be taken out, so that we are led to consider

$$\epsilon_u = \epsilon - \epsilon_{lam} = \frac{(\omega_1 - \omega_2)}{r_a d} J_{\omega, lam} (Nu_\omega - 1) = \frac{\nu^3}{d^4} \sigma^{-2} Ta (Nu_\omega - 1). \quad (6)$$

with the geometric parameter $\sigma = r_a^4/(r_1 r_2)^2$ denoted as quasi-Prandtl number. The dimensionless Taylor number is defined as $Ta = \sigma d^2 r_a^2 (\omega_1 - \omega_2)^2 / \nu^2$. Furthermore, the radius ratio is denoted by $\eta = r_1/r_2$ and the specific angular momentum is defined by $\mathcal{L} = r u_\varphi$.

To separate the influences of shear and rotation, we adopt the parameters introduced by Dubrulle et al. [10]. With the Reynolds numbers

$$Re_1 = \frac{r_1 \omega_1 d}{\nu} \quad \text{and} \quad Re_2 = \frac{r_2 \omega_2 d}{\nu}. \quad (7)$$

for the inner and outer cylinders, respectively, we form the shear Reynolds number and the rotation number

$$Re_S = \frac{2}{1 + \eta} (Re_1 - \eta Re_2) \quad \text{and} \quad R_\Omega = (1 - \eta) \frac{Re_1 + Re_2}{Re_1 - \eta Re_2}. \quad (8)$$

The relation to the Taylor number is given by $Ta = \sigma^2 Re_S^2$.

A comparison between (3) and (6) suggests an association $Pr \equiv \sigma$ between the Prandtl number Pr and the quasi-Prandtl number σ , and $Ra \equiv Ta$ between the Rayleigh number Ra and the Taylor

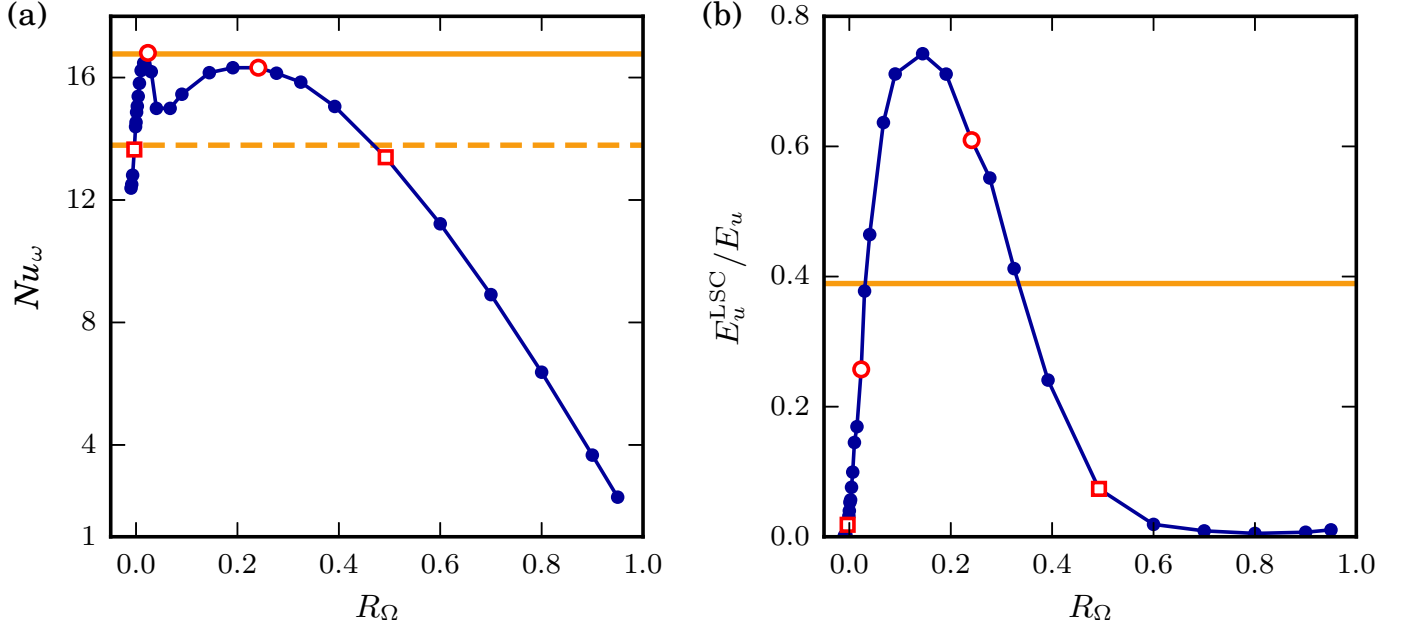


FIG. 1. (a) Variation of the Nusselt number with the system rotation R_Ω for TC flow with $\eta = 0.99$ and $Re_S = 2 \times 10^4$ (circles). (b) Ratio of the energy contained in the large-scale circulation E_u^{LSC} to the energy of the total cross-flow E_u as given in eq. (9). The horizontal lines in (a,b) indicate the corresponding values from RB convection with $Pr = 0.7$ and $Ra = 10^7$ (solid) and $Ra = 5 \times 10^6$ (dashed). The four possible TC data points for the comparison (with Nu_ω close to a RB Nusselt number) are marked as open symbols.

number Ta . However, there are various reasons why this is not sufficient. For example, a direct comparison between (3) and (6) suggests equality of the combinations $Pr^{-2}Ra$ and $\sigma^{-2}Ta$, only and does not relate Ra and Ta directly. Moreover, TC flow has two Reynolds numbers, and the Taylor number captures only their difference. The overall rotation, as measured by the rotation number R_Ω , does not enter, but it is known that the torque varies non-monotonically with R_Ω [3, 19, 22, 24, 27]. Similarly, critical values for the onset of instability are given by $Ra_c = 1708$ [8] for RB flow and by $Ta_c = 1708/[R_\Omega(1 - R_\Omega)]$ [10] for TC flow (in the limit $\eta \rightarrow 1$ where $Ta = Re_S^2$), again highlighting the significance of the rotation number. We therefore have to look for alternatives on how to relate the two flows.

III. CHOICE OF REFERENCE POINT FOR COMPARISON

In the following, we discuss how the reference point for the one-to-one comparison is chosen. As described above, equating Ra and Ta directly is not possible because of ambiguities in their definitions. A meaningful comparison can be based on the Nusselt number, because it defines the boundary layer thickness and hence the mean profiles. Similarly, the Reynolds stresses, when normalized by $Nu J_{lam}$,

should fluctuate with mean value 1 in regions where the viscous contributions to the transport are small. This allows for an absolute comparison of probability density functions since the dimensionless version with Nu scaled out has the same mean and, as we will show for one of the cases here, also the same variance.

We also have to select the curvature parameter η in TC flow, which has no counterpart in RB flow because the heated and cooled plates are planar. We therefore take $\eta = 0.99$ since the curvature effects disappear for η -values close to 1. Finally, the mean system rotation in TC flow which is defined by R_Ω has to be selected for the direct comparison. Again, an analogous parameter is missing in RB convection. In figure 1(a) a curve $Nu_\omega(R_\Omega)$ at $\eta = 0.99$ is shown for $Re_S = 2 \times 10^4$. A Nusselt number Nu_ω that is comparable to the RB flow value of $Nu_T = 16.7$ at $Ra = 10^7$ (solid horizontal line) was obtained for $R_\Omega = 0.023$ and $R_\Omega = 0.241$ (open circles). These two runs will be denoted as case 1 and case 2, respectively, and will be used to study the effects of the rotation number. In both cases the cylinders are co-rotating with angular velocity ratios $\mu = \omega_2/\omega_1 = 0.40$ and $\mu = 0.92$ for $R_\Omega = 0.023$ and $R_\Omega = 0.241$, respectively. Decreasing the Rayleigh number gives other crossing points, as indicated by the dashed line and the open squares in figure 1(a) for $Ra = 5 \times 10^6$. For this lower Ra the RB and TC flows differ noticeably, so that we will subsequently focus on the cases 1 and 2 only. We furthermore note that in the first case the relative distance to the linear instability $Ta/Ta_c \approx 5.35 \times 10^3$ is close to the corresponding RB value $Ra/Ra_c \approx 5.86 \times 10^3$ for $Ra = 10^7$, whereas in the second case the ratio $Ta/Ta_c \approx 4.29 \times 10^4$ is much higher.

Figure 1(b) shows the ratio

$$\frac{E_u^{LSC}}{E_u} = \frac{\langle \langle u_r \rangle_{\varphi,t}^2 + \langle u_z \rangle_{\varphi,t}^2 \rangle_{r,z}}{\langle u_r^2 + u_z^2 \rangle_{V,t}}, \quad (9)$$

of the energy contained in the mean vortical motion to the energy of the total cross-flow. It measures the relative strengths of temporally and streamwise-averaged Taylor vortices, which are analogous to the large-scale circulation in RB flow. The vortex strength varies with rotation, and the curve shows that case 2 is more strongly dominated by the large-scale vortices than case 1. In RB flow with $Ra = 10^7$, the corresponding energy ratio of approximately 0.4 is of similar magnitude and lies between the two TC cases.

As additional measures for the comparison of both flows, we analyse the boundary layer thicknesses. In analogy to the thermal boundary layer thickness $\delta_T = -\Delta/(2\partial_z \langle T \rangle|_{z=0,d}) = d/(2Nu_T)$ in RB flow, we define the boundary layer thicknesses at the inner cylinder ($r = r_1$)

$$\delta_\omega = \frac{\Delta_\omega}{-2\partial_r \langle \omega \rangle|_1} \quad \text{and} \quad \delta_{\mathcal{L}} = \frac{\Delta_{\mathcal{L}}}{-2\partial_r \langle \mathcal{L} \rangle|_1} \quad (10)$$

for the angular velocity and angular momentum profiles in TC flow with the total differences $\Delta_\omega = \omega_1 - \omega_2$ and $\Delta_{\mathcal{L}} = \mathcal{L}_1 - \mathcal{L}_2$. In the low-curvature case $\eta = 0.99$ analysed here, we also have $\delta_\omega \approx$

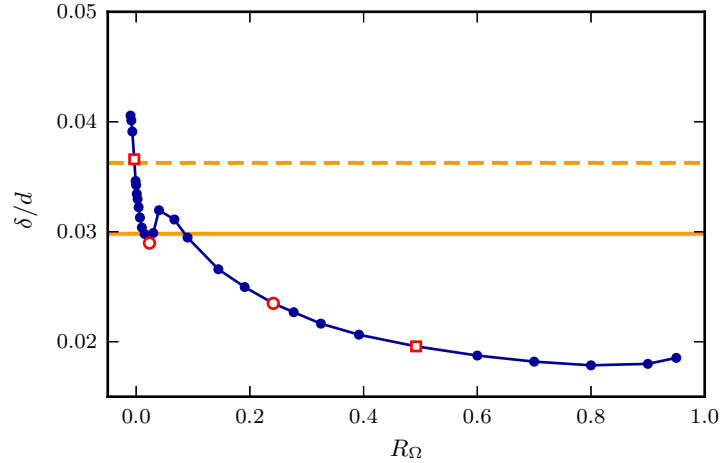


FIG. 2. The boundary layer thickness $\delta_{\mathcal{L}}$ which is based on the slope of the angular momentum profile at the wall is displayed versus R_{Ω} . The corresponding thermal boundary layer thickness $\delta_T = d/(2Nu_T)$ of the RB flow is indicated by the horizontal lines. Parameter values are $\eta = 0.99$ with $Re_S = 2 \times 10^4$ for TC flow and $Pr = 0.7$ with $Ra = 5 \times 10^6$ (dashed) and $Ra = 10^7$ (solid) for RB convection. The four possible TC data points for the comparison are again marked as open symbols.

$d/(2Nu_{\omega})$, whereas such a relation does not exist for $\delta_{\mathcal{L}}$. However, for strongly co-rotating cylinders δ_{ω} overestimates the width of the boundary layer region since then the angular velocity profiles have a significant slope in the bulk [3, 22]. As the angular momentum profile generally becomes almost flat in the bulk [5], the thickness $\delta_{\mathcal{L}}$ provides a better approximation to the size of the boundary layer region and will therefore be used here. In figure 2 the boundary layer thickness $\delta_{\mathcal{L}}$ is plotted for the same data as in figure 1(a). It is observed that the boundary layer thickness of case 1 matches almost perfectly with the thermal boundary layer thickness δ_T of the RB flow at $Ra = 10^7$. In case 2, the differences in the thickness scales are larger; here, the thickness $\delta_{\mathcal{L}}$ is smaller than $\delta_{\omega} \approx \delta_T = d/(2Nu_T)$ since the angular velocity profile is not flat in the central region. As we will see in the following, these differences will affect the statistical properties of the TC flows and thus the agreement with RB flow.

IV. STATISTICAL PROPERTIES

A. Mean vertical profiles

In figure 3 we compare the mean profiles of temperature to the mean profiles of the angular velocity $\omega = u_{\varphi}/r$ and the angular momentum $\mathcal{L} = ru_{\varphi}$. The upper row displays the comparison with the TC flow at the first local maximum at $R_{\Omega} = 0.023$ (case 1) (see figure 1a). The lower row repeats this

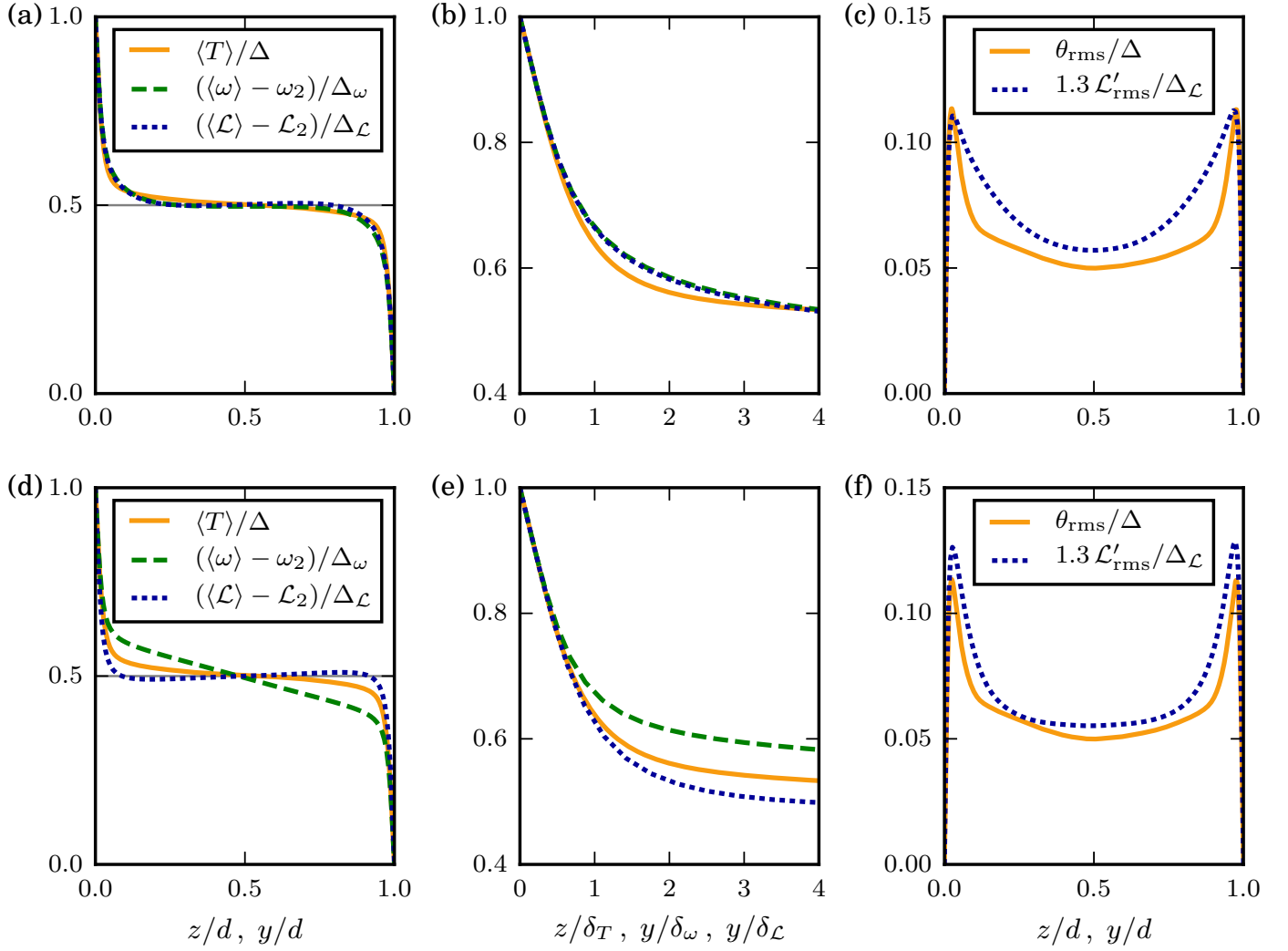


FIG. 3. (a) Profiles of the mean temperature $\langle T \rangle$ for $Pr = 0.7$ and $Ra = 10^7$ and of the mean angular velocity $\langle \omega \rangle$ and angular momentum $\langle \mathcal{L} \rangle$ for $\eta = 0.99$, $Re_S = 2 \times 10^4$ and $R_\Omega = 0.023$ (case 1). All profiles are rescaled to the interval $[0, 1]$ using $\Delta_\omega = \omega_1 - \omega_2$ and $\Delta_{\mathcal{L}} = \mathcal{L}_1 - \mathcal{L}_2$. The coordinate $y = r - r_1$ is used for the TC flow. (b) Magnification of the near-wall region. All coordinates are rescaled by the corresponding boundary layer thicknesses. (c) Profiles of the root mean square temperature and the root mean square angular momentum. The latter is rescaled by a factor of 1.3 for better comparability. (d,e,f) Similar comparison of the RB flow case to the TC flow run with $R_\Omega = 0.241$ (case 2).

comparison for the TC flow at the second local maximum in the $Nu_\omega - R_\Omega$ relation at $R_\Omega = 0.241$ (case 2). While the agreement with case 1 is very good, there are differences for case 2. Here, the angular velocity profile has a noticeable gradient in the central region, whereas the angular momentum is well mixed and lies closer to the temperature profile. From this comparison one can conclude that T is more closely associated with \mathcal{L} than with ω . Therefore, we compare the root mean square profiles of

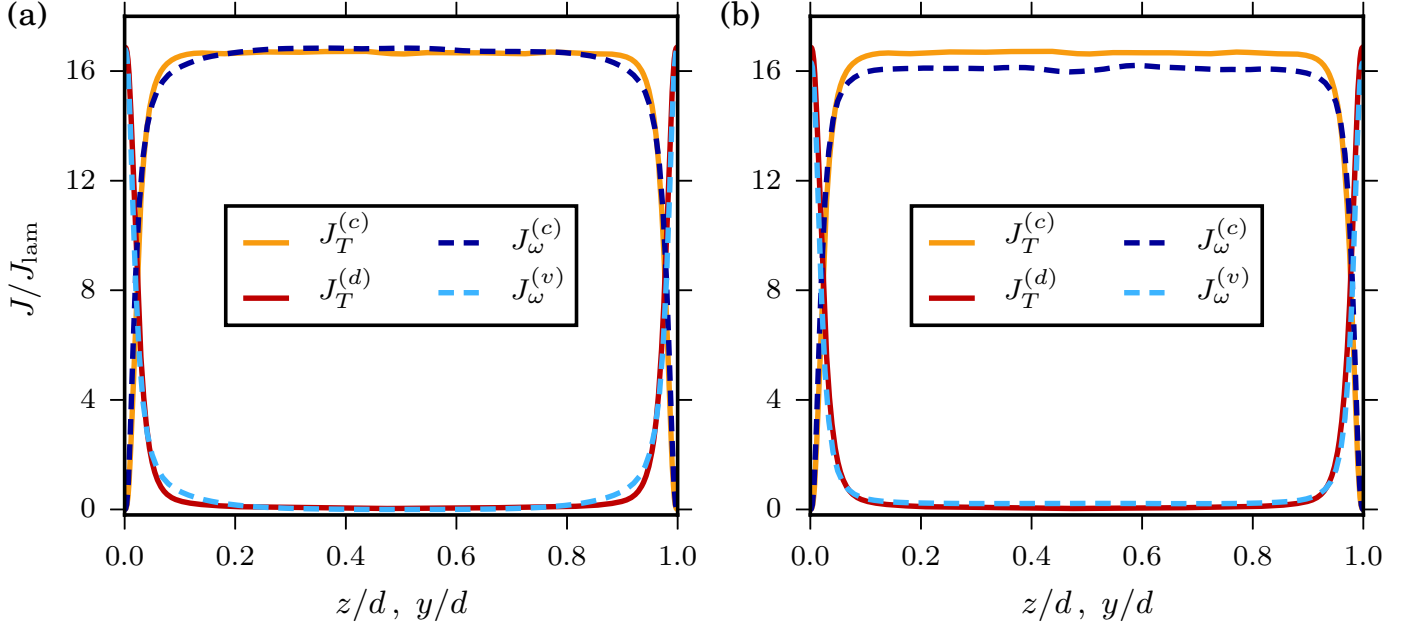


FIG. 4. Comparison between the contributions to the currents for (a) case 1 and (b) case 2 with the parameters described in figure 3. The convective and diffusive currents for the heat transport in RB are shown as continuous lines, the corresponding convective and viscous currents for the angular momentum transport in TC as dashed lines.

T and \mathcal{L} fluctuations in panels (c) and (f) of figure 3. The fluctuating fields are obtained by

$$\theta(\mathbf{x}, t) = T(\mathbf{x}, t) - \langle T \rangle(z), \quad (11)$$

$$\mathcal{L}'(\mathbf{x}, t) = \mathcal{L}(\mathbf{x}, t) - \langle \mathcal{L} \rangle(r). \quad (12)$$

For case 1, the peaks in $\mathcal{L}'_{\text{rms}}$ are broader than in case 2, which is consistent with the observation that the boundary layers are turbulent for case 1, but not for case 2 [4]. In the RB flow case, the boundary layer dynamics is close to laminar, and the peaks in θ_{rms} are narrower. Furthermore, we note that the shape of the root mean square angular velocity profile $\omega'_{\text{rms}} = \mathcal{L}'_{\text{rms}}/r^2$ (not shown here) hardly differs from $\mathcal{L}'_{\text{rms}}$ since the radius only varies by 1% for $\eta = 0.99$.

The heat flux in RB flow is decomposed into a convective and diffusive contribution which results in

$$J_T = J_T^{(c)}(z) + J_T^{(d)}(z) = \langle u_z T \rangle - \kappa \frac{\partial \langle T \rangle}{\partial z} = Nu_T J_{T, \text{lam}}. \quad (13)$$

A similar decomposition into a convective and viscous contribution in the TC flow case leads to

$$J_\omega = J_\omega^{(c)}(r) + J_\omega^{(v)}(r) = r \langle u_r \mathcal{L} \rangle - \nu r^3 \frac{\partial \langle \omega \rangle}{\partial r} = Nu_\omega J_{\omega, \text{lam}}. \quad (14)$$

Figure 4 displays the vertical (radial) profiles. Panel (a) compares with case 1 while panel (b) compares with case 2. As expected the dissipative contributions are significant in the boundary layers and

become small in the bulk. The convective parts dominate the bulk and drop to zero at the walls due to the no-slip boundary conditions. Furthermore, the sum of both transport contributions remains constant across the whole layer in both systems. It can be seen again that profiles of case 1 show better agreement with RB flow than the profiles of case 2. Since in the latter case the angular velocity profile is not flat in the central region (cf. figure 3d), the viscous contribution $J_\omega^{(v)}$ is larger than the corresponding diffusive part $J_T^{(d)}$, which additionally results in a smaller convective contribution $J_\omega^{(c)}$.

B. Probability density functions

We now refine the analysis and report the statistics of the convective currents in averaging surfaces at different distance from the inner (bottom) wall. First, it is important to note that only the temperature and angular momentum fluctuations θ and \mathcal{L}' that deviate from the corresponding mean profile contribute to the net transport through the averaging surfaces, since $\langle u_z \rangle = \langle u_r \rangle = 0$ by incompressibility, and therefore $\langle u_z T \rangle = \langle u_z \theta \rangle$ and $r \langle u_r \mathcal{L} \rangle = r \langle u_r \mathcal{L}' \rangle$. Therefore, we study the local convective currents based on the fluctuations θ and \mathcal{L}' instead of the total fields. Figure 5 compares the probability density functions (PDFs) of the local convective angular momentum current $j_\omega^{(c)} = r u_r \mathcal{L}'$ for cases 1 (top row) and 2 (bottom row) with the local convective heat current $j_T^{(c)} = u_z \theta$ for planes at different distances from the wall. All quantities are normalized by the corresponding mean currents J_ω and J_T . In all cases, it is observed that the skewness of the distributions increases with the distance of the analysis surface from the inner (bottom) wall. The net convective transport has to be positive, and its share of the total transport increases towards the bulk. It is also observed that the tails of the PDFs of TC flow for case 2 deviate strongly from the ones for RB flow away from the boundary layer.

The trend is different for the comparison of case 1 with RB flow. While the largest differences arise for the data at $4\delta_{\mathcal{L}}$, the agreement is very good for the data taken at $\delta_{\mathcal{L}}$ and r_a . The region just above the boundary layer thickness is dominated by rising plumes and recirculations next to the plumes. It is sometimes also denoted as the plume mixing layer [7]. The reason for the differences in the width of the tails in panels (b) and (e) of figure 5 could therefore be related to the shape of the plumes and the frequency of their detachment, which differ between RB and TC flow as will be shown in the next subsection.

The observation that the local fluctuations in case 2 are enhanced compared to case 1 can be understood by analysing the components that form $j_\omega^{(c)} = r u_r \mathcal{L}'$. Since the fluctuation amplitude of \mathcal{L}' varies little between both cases (cf. figure 3(c,f)), and the radius r remains unchanged, the difference must occur in the radial velocity u_r . In [5] it was shown that the fluctuation amplitude $(u_r)_{\text{rms}}$ varies with mean rotation (R_Ω) and in case 2 it is twice as large as in case 1. This increase is partly caused

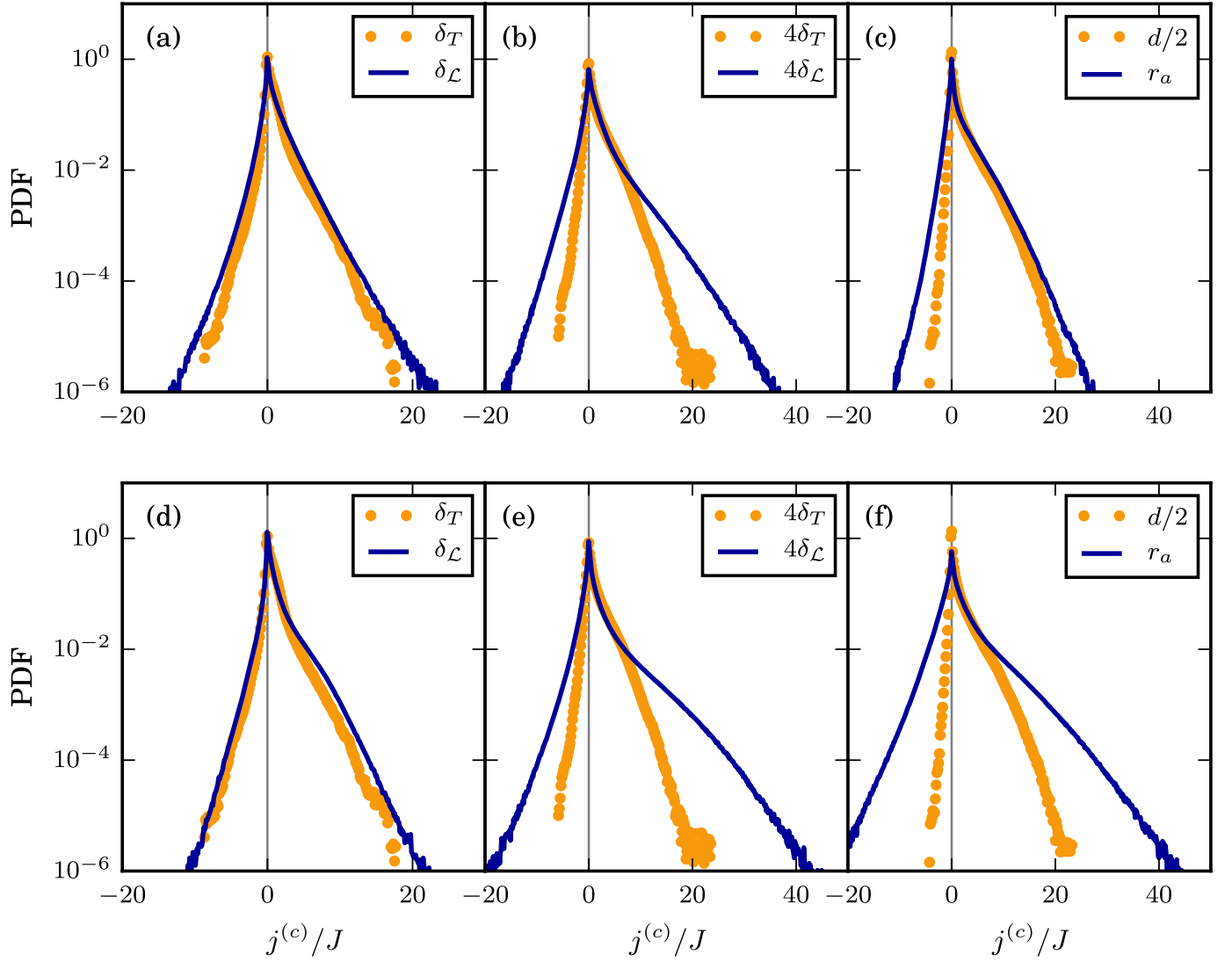


FIG. 5. Probability density functions (PDFs) of the local convective currents $j_T^{(c)} = u_z \theta$ (filled circles) and $j_\omega^{(c)} = r u_r \mathcal{L}'$ (solid lines) computed at the boundary layer thickness δ_T ($\delta_{\mathcal{L}}$) in panels (a, d), at $4\delta_T$ ($4\delta_{\mathcal{L}}$) in panels (b, e) and at the centre $d/2$ (r_a) in panels (c, f). The local currents are normalized by the corresponding total mean currents J_T and J_ω . Panels (a, b, c) are for case 1 and panels (d, e, f) are for case 2 for the same parameters as in figure 3. Here $\theta = T - \langle T \rangle$ and $\mathcal{L}' = \mathcal{L} - \langle \mathcal{L} \rangle$ denote the fluctuations around the corresponding time- and area-averaged profiles.

by a strengthening of the mean Taylor vortices, cf. figure 1(b). The stronger u_r fluctuations result in wider tails in figure 5(e,f) but do not significantly affect the distribution at $\delta_{\mathcal{L}}$ where the radial velocity is restricted due to the proximity of the cylinder wall.

In figure 6 we compare individual components of the transport currents of angular momentum and heat. They are u_z and θ in the RB case, and the radial velocity u_r and angular momentum \mathcal{L}' in TC flow. It can be observed that the agreement between case 1 and the RB flow is good. For case

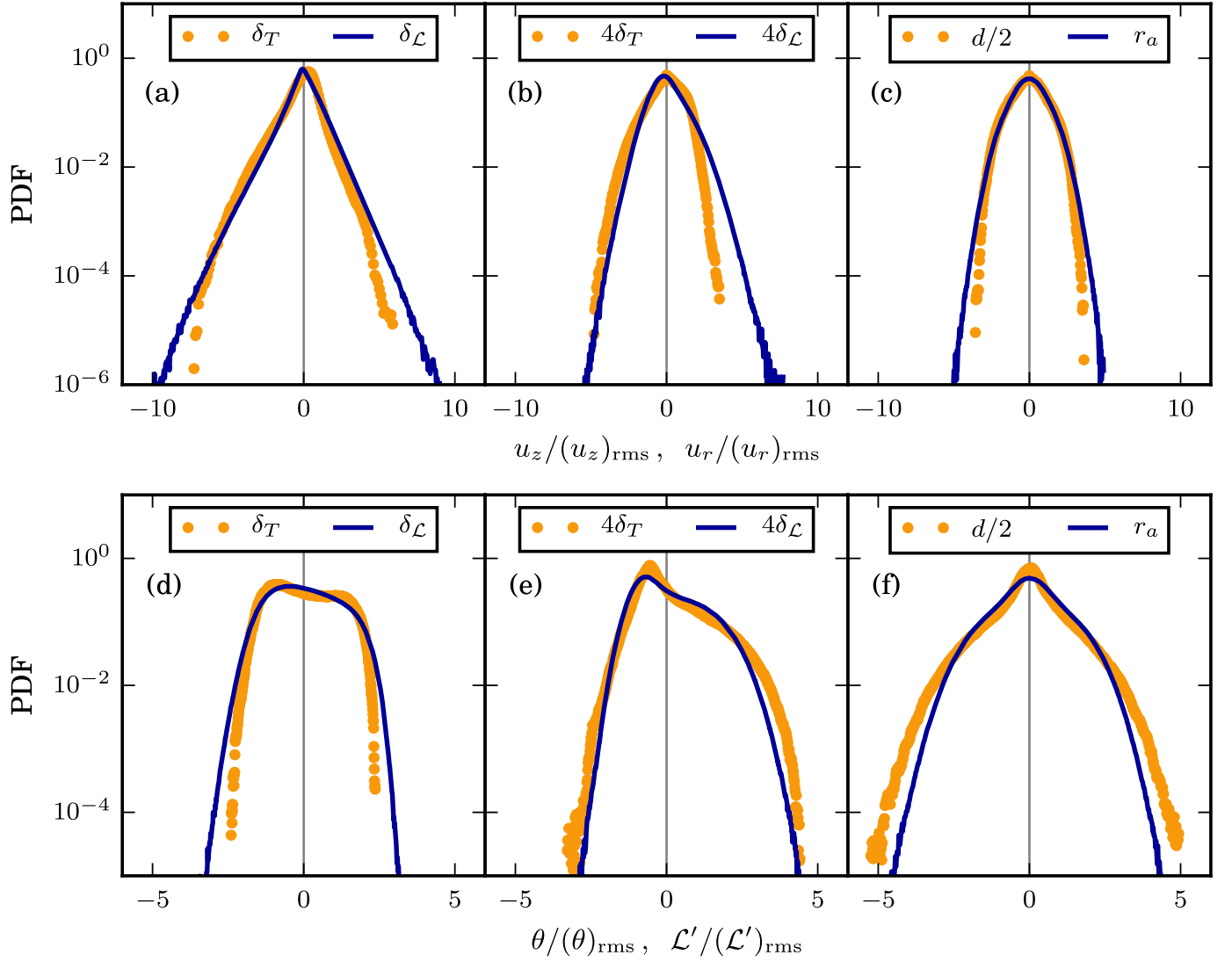


FIG. 6. Comparison of the PDFs of individual components of the turbulent fields. All data are for case 1 and the RB flow. In the upper row, the PDFs of the axial velocity u_z (RB, filled circles) and radial velocity u_r (TC, solid lines) are compared, in the lower row the PDFs of the temperature θ (RB, filled circles) and angular momentum \mathcal{L}' (TC, solid lines). Data are obtained for δ_T ($\delta_{\mathcal{L}}$) in panels (a, d), at $4\delta_T$ ($4\delta_{\mathcal{L}}$) in panels (b, e) and at the centre $d/2$ (r_a) in panels (c, f). Each PDF is normalized by its corresponding root mean square value.

2 (not shown here), the deviations of the individual PDFs of θ and \mathcal{L}' were larger. In a turbulent flow one expects Gaussian statistics for the individual components of the velocity field. In figure 6(a) exponential tails are observed for the PDFs of u_z and u_r at the height of (thermal) boundary layer thickness. This is a clear statistical fingerprint for an enhanced intermittency in the near-wall region which is connected with the plume formation. Also, in figure 6(b) a fatter tail for the radial component is detected which confirms our observation in figure 5(b).

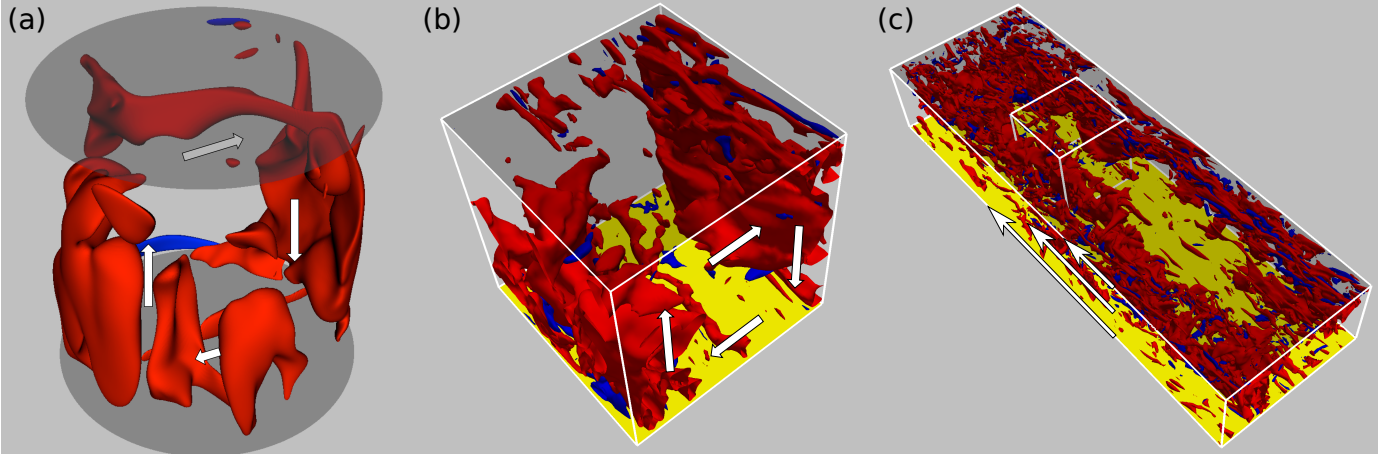


FIG. 7. Isosurface snapshots of the convective transport currents $j_T^{(c)}$ for RB flow and $j_\omega^{(c)}$ for TC flow (case 1). Isolevels $j^{(c)}/J = -3$ (blue) and 3 (red) are shown. (a) RB flow with top and bottom walls indicated by semi-transparent planes. (b,c) TC flow with the inner and outer cylinder indicated by a yellow and semi-transparent surface, respectively. (b) Magnification of the segment marked in (c) with an extension of $1d$ in each direction, to match the aspect ratio of the RB flow domain. (c) Simulated fraction of the annular domain. The arrows indicate the large-scale circulation in (a), the Taylor vortex in (b) and the velocity profile in (c).

The distributions of the temperature and angular momentum fluctuations (see lower row of figure 6) are skewed and take a symmetric shape in the midplane only as shown in figure 6(f). For all three distances the tails of both PDFs are in very good agreement. The distribution in the midplane is again not Gaussian which has been reported already in [14]. The specific cusp-like form around the origin and the increasingly pronounced exponential tails in the PDF of temperature fluctuations have been discussed, for example, by Yakhot on the basis of a hierarchy of momentum equations for the temperature fluctuations [29]. Interestingly, even such specific details of the small-scale statistics prevail in our comparison between RB and TC flow.

C. Relation between transport and flow structures

In the last subsections, we identified small differences in the statistical properties of the RB flow and case 1 of TC flow and attributed them to differences in the flow structures. The spatial organization of currents is shown in figure 7, where isosurfaces of the convective current (the top row of figure 5) for the levels $j^{(c)}/J = \pm 3$ are plotted. Panels (a) and (c) show the full simulation domains in both cases. The magnification in figure 7(b) displays a section of the TC flow with the same aspect ratio as the RB domain in panel (a). Since the net transport current is positive, on average, there is a larger volume

fraction of red isosurfaces than blue ones. The large coherent regions of high convective current, which occur near the sidewall in panel (a) and near the left and right surfaces in panel (b), coincide with the upward and downward motion of the large-scale circulation in RB and a Taylor vortex in TC (see white arrows in panels (a,b)). Consequently, the positive tails in figure 5(c) are related to this large-scale motion. The similarity in the large-scale organization of the currents explains why the differences in geometry (cylindrical vs. rectangular domain) have a minor influence on the statistical properties in the middle, cf. figure 5(c). The isosurfaces of the TC flow are more fragmented and less smooth than for the RB flow, which indicates a higher level of fluid turbulence in the system. Quantitatively, we find in RB flow for the large-scale Reynolds number $Re_{rms} = u_{rms}d/\nu = 675$, with the root mean square velocity u_{rms} calculated from all three velocity components in the entire cell [26]. This is significantly smaller than the corresponding Reynolds numbers in TC flow (with the mean rotation subtracted), which are $Re_{rms} = 2251$ and $Re_{rms} = 2712$ for the cases 1 and 2, respectively. It can thus be expected that the boundary layers in the RB case are still close to laminar, while the ones in case 1 of TC flow are already turbulent [4]. Specifically, we find for the boundary-layer Reynolds numbers, defined based on the boundary layer thickness and shear across the boundary layer, values of ~ 30 for RB flow [26] and of ~ 300 and ~ 200 for the TC cases 1 and 2, respectively [4]. The turbulent fluctuations in the TC boundary layer account for the deviations in the tails of the PDFs and the slight deviations in the area-averaged profiles, in particular at the heights of $z = 4\delta_T$ and $y = 4\delta_L$, respectively, in figure 5(b).

V. CONCLUSIONS

In the present work we discussed a direct comparison of the statistical properties of Rayleigh–Bénard (RB) convection and Taylor–Couette (TC) flow. The comparison is motivated by analogies of dimensionless system parameters (such as Rayleigh and Taylor numbers), the same form of the energy balances, (3) and (6), and the similarities in the currents of heat and angular momentum (see also references [2, 11–13]).

Our study shows that the operating point for a specific comparison between TC and RB flows can be determined by choosing corresponding values of Nusselt numbers since the Nusselt number defines the boundary layer thickness and hence the transport properties. We also find that a better characterization of TC flow can be based on the pair of shear Reynolds and rotation numbers, (Re_S, R_Ω) , than on Taylor and quasi-Prandtl numbers, (Ta, σ) , since the latter do not reflect the mean rotation of the cylinders. We demonstrated that for sufficiently large shear Reynolds number Re_S , multiple TC flow cases at different rotation numbers can have the same Nusselt number as RB convection, i.e.

the same amount of angular momentum is transported between the cylinders in TC flow as heat from the bottom to the top in the RB case. The comparison also shows that the case with the smaller rotation number R_Ω (case 1) provides a better agreement with RB flow than the case of larger rotation number. For this pair of flows, a remarkable agreement between mean profiles as well as probability density functions of fluctuating quantities is found.

Studies of the mean profiles and the PDFs of the convective currents show that the differences between RB flow and TC flow case 1 are most pronounced in the mixing layer above the (thermal) boundary layer. They can be attributed to the strong fluctuations in this region which are connected with the detachment of plumes and other differences in the dynamics: the boundary layers in the convection case are still very close to being laminar, but in the TC system they are already turbulent. The differences should, therefore, become smaller when the boundary layers in RB become turbulent as well.

The TC flow case 2, which is characterized by a larger mean rotation (R_Ω), shows greater differences to the RB case. As a consequence of rotation, the angular velocity profile has a significant gradient in the central region, which results in a higher (lower) dissipative (convective) transport current than in the RB case. Furthermore, enhanced radial velocity fluctuations and stronger mean Taylor vortices occur for case 2 and lead to broader PDFs of the convective current away from the boundary layer, which differ from the heat flux distributions in RB flow. This demonstrates that the mean rotation determines how well the transport characteristics of TC and RB flow are comparable.

The comparison presented here shows that for judiciously chosen pairs of parameters in RB and TC flow one can actually relate their transport properties in detail, both in the mean and in the fluctuations, thereby confirming the analogies between the *twins of turbulence* [6] for a larger set of properties.

ACKNOWLEDGMENTS

We would like to thank M. S. Emran and R. du Puits for scientific discussions at the beginning of this work. JS acknowledges computational resources provided by the John von Neumann Institute for Computing within Supercomputing Grant HIL09. HB and BE thank M. Avila for providing the code used for the TC simulations and acknowledge computational resources at the LOEWE-CSC in Frankfurt. The paper was written during a workshop at the Lake Arrowhead Conference Center, and BE and JS would like to thank the Institute of Pure and Applied Mathematics (IPAM) of the

University of California Los Angeles for financial support.

- [1] G. Ahlers, S. Grossmann, and D. Lohse. Heat transfer and large scale dynamics in turbulent Rayleigh–Bénard convection. *Rev. Mod. Phys.*, 81:503–537, 2009.
- [2] P. Bradshaw. The analogy between streamline curvature and buoyancy in turbulent shear flow. *J. Fluid Mech.*, 36:177–191, 1969.
- [3] H. J. Brauckmann and B. Eckhardt. Direct numerical simulations of local and global torque in Taylor–Couette flow up to $Re = 30\,000$. *J. Fluid Mech.*, 718:398–427, 2013.
- [4] H. J. Brauckmann and B. Eckhardt. Marginally stable and turbulent boundary layers in low-curvature Taylor–Couette flow. *J. Fluid Mech. (submitted)*, arXiv:1609.00556, 2016.
- [5] H. J. Brauckmann, M. Salewski, and B. Eckhardt. Momentum transport in Taylor–Couette flow with vanishing curvature. *J. Fluid Mech.*, 790:419–452, 2016.
- [6] F. H. Busse. The twins of turbulence research. *Physics*, 5:4, 2012.
- [7] B. Castaing, G. Gunaratne, F. Heslot, L. Kadanoff, A. Libchaber, S. Thomae, X. Z. Wu, Zaleski S., and G. Zanetti. Scaling of hard thermal turbulence in Rayleigh–Bénard convection. *J. Fluid Mech.*, 204:1–30, 1989.
- [8] S. Chandrasekhar. *Hydrodynamic and Hydromagnetic Stability*. Clarendon Press, 1 edition, 1961.
- [9] F. Chillà and J. Schumacher. New perspectives in turbulent Rayleigh–Bénard convection. *Eur. Phys. J. E*, 35:58, 2012.
- [10] B. Dubrulle, O. Dauchot, F. Daviaud, P.-Y. Longaretti, D. Richard, and J.-P. Zahn. Stability and turbulent transport in Taylor–Couette flow from analysis of experimental data. *Phys. Fluids*, 17:095103, 2005.
- [11] B. Dubrulle and F. Hersant. Momentum transport and torque scaling in Taylor–Couette flow from an analogy with turbulent convection. *Eur. Phys. J. B*, 26:379–386, 2002.
- [12] B. Eckhardt, S. Grossmann, and D. Lohse. Fluxes and energy dissipation in thermal convection and shear flows. *Europhys. Lett.*, 78:24001, 2007.
- [13] B. Eckhardt, S. Grossmann, and D. Lohse. Torque scaling in turbulent Taylor–Couette flow between independently rotating cylinders. *J. Fluid Mech.*, 581:221–250, 2007.
- [14] M. S. Emran and J. Schumacher. Fine-scale statistics of temperature and its derivatives in convective turbulence. *J. Fluid Mech.*, 611:13–34, 2008.

- [15] P. F. Fischer. An overlapping Schwarz method for spectral element solution of the incompressible Navier–Stokes equations. *J. Comput. Phys.*, 133:84–101, 1997.
- [16] S. Grossmann, D. Lohse, and C. Sun. High–Reynolds number Taylor–Couette turbulence. *Annu. Rev. Fluid Mech.*, 48:53–80, 2016.
- [17] E. L. Koschmieder. *Bénard Cells and Taylor Vortices*. Cambridge University Press, 1993.
- [18] A. R. Low. Instability of viscous fluid motion. *Nature*, 115:299–300, 1925.
- [19] S. Merbold, H. J. Brauckmann, and C. Egbers. Torque measurements and numerical determination in differentially rotating wide gap Taylor–Couette flow. *Phys. Rev. E*, 87:023014, 2013.
- [20] A. Meseguer, M. Avila, F. Mellibovsky, and F. Marques. Solenoidal spectral formulations for the computation of secondary flows in cylindrical and annular geometries. *Eur. Phys. J. Spec. Top.*, 146:249–259, 2007.
- [21] Nek5000 Homepage. <https://nek5000.mcs.anl.gov>.
- [22] R. Ostilla, R. J. A. M. Stevens, S. Grossmann, R. Verzicco, and D. Lohse. Optimal Taylor–Couette flow: direct numerical simulations. *J. Fluid Mech.*, 719:14–46, 2013.
- [23] R. Ostilla-Mónico, E. P. van der Poel, R. Verzicco, S. Grossmann, and D. Lohse. Exploring the phase diagram of fully turbulent Taylor–Couette flow. *J. Fluid Mech.*, 761:1–26, 2014.
- [24] M. S. Paoletti and D. P. Lathrop. Angular momentum transport in turbulent flow between independently rotating cylinders. *Phys. Rev. Lett.*, 106:024501, 2011.
- [25] J. D. Scheel, M. S. Emran, and J. Schumacher. Resolving the fine-scale structure in turbulent Rayleigh–Bénard convection. *New J. Phys.*, 15:113063, 2013.
- [26] J. D. Scheel and J. Schumacher. Local boundary layer scales in turbulent Rayleigh–Bénard convection. *J. Fluid Mech.*, 758:344–373, 2014.
- [27] D. P. M. van Gils, S. G. Huisman, G.-W. Bruggert, C. Sun, and D. Lohse. Torque scaling in turbulent Taylor–Couette flow with co- and counterrotating cylinders. *Phys. Rev. Lett.*, 106:024502, 2011.
- [28] F. Wendt. Turbulente Strömungen zwischen zwei rotierenden konaxialen Zylindern. *Ing.-Arch.*, 4:577–595, 1933.
- [29] V. Yakhot. Probability distributions in high–Rayleigh number Bénard convection. *Phys. Rev. Lett.*, 63:1965–1967, 1989.